

1 **A High Dense Temperature-Salinity Dataset Observed by**
2 **AutomaticAutonomous Underwater Vehicles toward Mesoscale**
3 **eddies' Evolutions and Associated Submesoscale Processes in**
4 **South China Sea**

5 Chunhua Qiu^{1,2}, Zhenyang Du^{1,2}, ~~Jianheng Yu³~~, ~~Huabin Mao⁴~~, Haibo Tang^{1,2}, Zhenhui Yi^{1,2},
6 Jiawei Qiao^{1,2}, Dongxiao Wang^{1,2,*}, Xiaoming Zhai^{3~~5~~}, ~~Yejiang Shu⁴~~ Wenbo Wang^{1,2}

7 1. School of Marine Sciences, State Key Laboratory of Environmental Adaptability for Industrial
8 Products, Sun Yat-Sen University, and Southern Marine Science and Engineering Guangdong
9 Laboratory (Zhuhai), Zhuhai, China

10 2. Guangdong Provincial Key Laboratory of Marine Resources and Coastal Engineering, School of
11 Marine Sciences, Sun Yat-sen University, Guangzhou 510275, China

12 ~~3. State Key Laboratory of Robotics, Shenyang Institute of Automation, Chinese Academy of Sciences,~~
13 ~~Shenyang 110016, China~~

14 ~~4. State Key Laboratory of Tropical Oceanography, South China Sea Institute of Oceanology, Chinese~~
15 ~~Academy of Sciences, Guangzhou, China~~

16 ~~5. Centre for Ocean and Atmospheric Sciences, School of Environmental Sciences, University of East~~
17 ~~Anglia, Norwich, UK~~

18
19
20 **Corresponding author:**

21 Dongxiao Wang

22 School of Marine Sciences,

23 Sun Yat-sen University

24 Email: dxwang@mail.sysu.edu.cn

25

26

27 **Abstract.** Marginal seas are usually fulfilled with strongly varying mesoscale eddies
28 (MEs), which evolutions plays vital roles in regulating global oceanic energy
29 equilibrium, triggering submesoscale processes with strong vertical velocity, and
30 inducing high biogeochemistry transport. But the temporal evolutions of MEs and
31 submesoscale processes with several kilometers' resolutions are difficult to be
32 measured by traditional observations with passive working mode. The **automatic**
33 underwater gliders (**AUGUGs**) and vehicles (AUVs) positively observe oceanic motion,
34 and could provide us spatiotemporal synchronization information for strongly varying
35 MEs. Here, we present a 9-year high dense dataset of AUVs/**AUGUGs** observations in
36 2014-2022 in the South China Sea (SCS) can be downloaded from
37 <https://doi.org/10.57760/sciencedb.11996> (Qiu et al., 2024b). Totally, 9 **AUGUG** and 2
38 AUV cruise experiments were conducted, and 50 **AUGUGs** (2 AUVs) equipment were
39 deployed with zonal and temporal resolutions of < 7 km and <6 hour. It covers the area
40 of eddy's birth, propagation, and dissipation, presenting us the most complete data to
41 investigate the evolution of MEs at different life stages. 40% of them reach resolutions
42 < 1 km and < 1 hour, which provides us the dynamic characteristics of submesoscale
43 instabilities across and along front at the eddy edge. This dataset has potential in
44 improving the forecast accuracy in physical and biogeochemistry numerical model.
45 Much more aggressive field investigation programs will be promoted by the NSFC in
46 future.

47

48 Keywords: **AutomaticAutonomous** Underwater Vehicles; Mesoscale eddies;
49 submesoscale processes; South China Sea

50

51 1. Background

52 Evolutions of mesoscale eddies (MEs), with high geostrophic straining, favors the
53 generation of submesoscale processes with several kilometers' spatial resolution
54 (McWilliam, 2016), and requires high-accuracy, spatiotemporal synchronization and
55 dense observations. Marginal seas (such as, Gulf of Mexico, South China Sea,
56 Mediterranean) are usually fulfilled with ~~multi-scale oceanic motions, i.e. boundary~~
57 ~~current, mesoscale eddie~~MEs (MEs; Rossby number $R_o = U/fL \approx 0.1$), and smaller
58 scale processes ($R_o > 1$). MEs, with spatial scale of 50–300 km and temporal scale of
59 several weeks to months, play vital roles in the transport of matter and energy (Chelton
60 et al., 2007; Morrow et al., 2004). They are numerous in the global ocean and also in
61 the tropical marginal sea of South China Sea (SCS; Chen et al., 2011; Wang et al., 2003;
62 Xiu et al., 2010). They easily generate by obtaining kinetic energy from large-scale
63 current, and easily dissipate to submeso- or smaller- scale processes at the slope region
64 via shear and baroclinic instabilities (Oey, 1995; Okkonen et al., 2003).

65 Observation plats for MEs include ship-cruise, satellite, Argo float, mooring,
66 drifters, ~~automatic~~autonomous unmanned vehicle (AUV), and ~~automatic~~ underwater
67 gliders (AUGUG), etc. These plats have been utilized to detect variations of MEs in
68 SCS (Table 1). Ship-cruise observations are the most traditional methods to investigate
69 the MEs' general structures (Wang et al., 1987; Xu et al., ~~1996~~1997), but difficult to
70 track their spatiotemporal evolutions. Satellite data provide wide surface information
71 of MEs (i.e., temporal and spatial scales; Chelton et al., 2011) and air-sea interactions
72 have been revealed (Ni et al., 2021). Southwest of Taiwan Islands, northwest of Luzon
73 Islands, Xisha Islands region, and east of Vietnam are the four main eddy birth pools
74 (Hwang et al., 2000; Wang et al., 2003; Nan et al., 2011). After birth, MEs move
75 westward, southwestward, or northwestward under the control of the first-baroclinic
76 Rossby wave (Lin et al., 2007; Xiu et al., 2010; Chen et al., 2011). Since 2002, a large
77 number of Argos have been deployed, providing routine measurements to describe
78 vertical structures of MEs (He et al., 2018; Table 1). The spatiotemporal resolutions of
79 Argo profiles are approximately 100 km and 10 days, which is difficult to capture the

80 high-frequency variability of MEs and submesoscale processes (Table 1).

81

Table 1. Observation studies of ME in SCS.

82

ME: mesoscale eddies; SCS: South China Sea

Ship Observation (CTD Station)	Dale, 1956	Cool pool near Vietnam
	Wang et al., 1987	Warm eddy near southwestern of Taiwan Islands
	Xu et al., 1996 1997 ;	Northwest of Luzon Islands, named Luzon cold eddy
	Li et al., 1998	A warm eddy in northeast of NSCS
	Chu et al., 1998	An eddy pair in central of SCS.
	Fang et al., 2002	Vietnam warm eddy
Satellite Observations (sea level anomaly; velocity)	Hwang et al., 2000; Wang et al., 2003; Nan et al., 2011 ^a	Topex/Poseidon altimeter data, 94 cold eddy, 124 warm eddy. Southwest of Taiwan Islands, northwest of Luzon Islands, East of Vietnam.
	Lin et al., 2007; Chen et al., 2011; Xiu et al., 2010	Radius, life cycle, tracking, seasonal and interannual variations of mesoscale eddies
	He et al., 2016	The role of ENSO on interannual variation in Luzon Strait mesoscale eddies
	He et al., 2019	MEs' influence on Chl-a
Argo; Mooring	Li et al., 2022	Vertical tilt of Mesoscale eddy
	He et al., 2018	Reconstruction data combine altimeter and Argos, revisit the three-dimensional structures of ME
	Zhang et al., 2017	By using mooring array, investigate eddy looping from Luzon Strait

83

84 Attributed to the positively track, AUVs and AUGUGs become more and more
 85 important tools in exploring marine environment over last two decades, due to the
 86 advantages of low cost, long-duration, controllability and reusability. Our group has
 87 collected dense UGs and AUVs observations across MEs. UGs adjust buoyancy to
 88 generate gliding motion through water columns by a pair of wings, and hybrid
 89 underwater gliders have been developed since 2004 (Bachmayer et al., 2004; Caffaz et
 90 al., 2010). Many international products of AUGUGs were operated, such as “Seaglider”
 91 (Eriksen et al., 2001), “Spray” (Sherman et al., 2001), “Slocum” (Webb et al., 2001),
 92 “Deepglider” (Osse and Eriksen, 2007), “SeaExplorer”. Their UGs' product companies
 93 and related information are listed in Table 2. UGs moves in a sawtooth trajectory at a

slow speed of 0.3 m/s, while AUVs are propeller-driven, acting as sawtooth and drifting mode at the maximum speed of 1 m/s (Hobson et al., 2012). It takes around 8/3 days for a UG/AUV to pass a quasi-steady eddy with mean radius of ME (100 km) in SCS. Kinds of sensors, such as, conductivity-temperature-depth(CTD), GPS are installed on the UGs and AUVs to measure marine environment. Hence, Multi-year AUGUGs and AUVs have been successfully used in detecting strongly varying features in some marginal seas, such as estimation of trends of Gulf Stream (Todd and Ren, 2023), the water mass exchanges between Bay of Bengal and Arabian Sea (Rainville et al., 2022). We reported AUGUGs experiments since 2014 (Qiu et al., 2015), and made AUV experiments since 2018 (Huang et al., 2019; Qiu et al., 2020). Here, we present 9-year (2014-2022) AUVs and AUGUGs datasets in SCS, and try to show their potential abilities in detecting the evolutions of MEs and the associated submesoscale processes.

Table 2. Types of several popular UGs (underwater gliders)

Types	Development Organizations
Seaglider	University of Washington
Spray	Scripps Institute of Oceanography and Woods Hole, https://spray.ucsd.edu/pub/rel/info/spray_description.php
Slocum serials	Webb Research Cor.
Deepglider / Oculus	Kongsberg Underwater Technology, Inc.
SeaExplorer glider	ACSA, Sep.5, 2013 https://www.marinetechologynews.com/news/seaexplorer-underwater-glider-record-487228
Sea Wing	Shenyang Institute of Automation, Chinese Academy of Sciences https://baike.baidu.com/item/%E6%B0%B4%E4%B8%8B%E6%BB%91%E7%BF%94%E6%9C%BA/4560334
Petrel	Tianjin University; https://baike.baidu.com/item/%E2%80%9C%E6%B5%B7%E7%87%95%E2%80%9D%E5%8F%B7%E6%B0%B4%E4%B8%8B%E6%BB%91%E7%BF%94%E6%9C%BA/13977071

2. Data Description

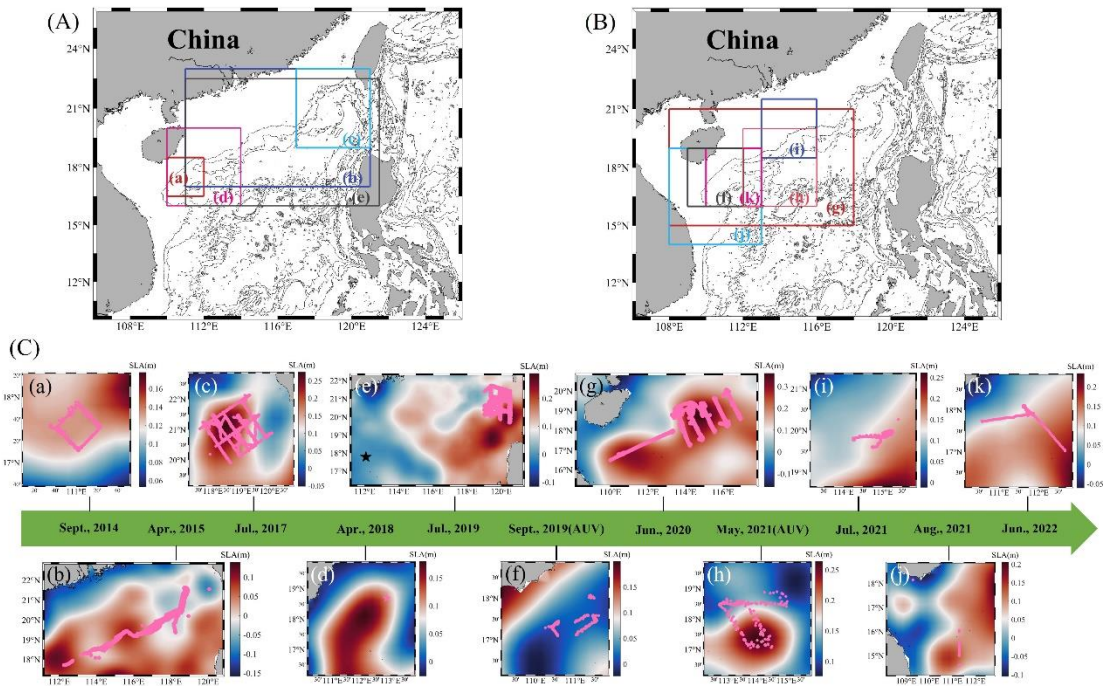
2.1 AUGUG and AUV experiment sites

Different with Rainville et al (2022) and Todd and Ren (2023), most of our experiments aimed to detect the evolution of MEs or submesoscale processes. Two products of Chinese AUGUGs named “Sea Wing” and “Petrel” are utilized in revealing the development of MEs in this study. Since 2014, we have conducted 11 experiments,

114 totally collecting 24498 temperature and salinity profiles, which is even more than those
115 in Gulf Stream (Todd and Ren, 2023). 50 AUGUGs and 2 AUVs were deployed in
116 northern SCS. The deploying time, installed sensors, and diving depths of
117 AUGUGs/AUVs experiment were shown in Table 3. More detailed information,
118 including vehicle serial number, waypoints, matching time, latitude, and longitude is
119 stored in the data with *.NC format. The gray highlighted the AUGUG network
120 experiments, with number of AUGUGs ≥ 3 . Such as, in the experiments of 2017, 2019
121 and 2020, more than 10 AUGUGs were deployed to detect the three-dimensional
122 structures of the mesoscale eddies. The largest AUGUG network was conducted in 2021,
123 including 50 AUGUGs, which was set to investigate eddy-current interaction.
124

Table 3. Information of individual AUGUG/AUV experiment and the observing purpose.
ME: Mesoscale Eddies; AUV: Autonomous Underwater Vehicle; UG: Underwater Glider.

Number	Equipment	Time	Number of Qualified Profiles	Number of Eliminated Profiles (Stage)	Number of equipment	Sensor of equipment (*: with Shipped CTD; #: with DO and CH-a sensors; ++: Velocity)	Diving depth of equipment	Observing Purpose
1	AUGUG	Sept. 19- Oct. 15, 2014; 26 days	227	0	1 AUGUG	Seabird Glider Payload CTD(GPCTD)	1000 m	Mixed layer heat budget; sea trials
2	AUGUG	Apr. 18-Jul. 6, 2015; 78 days	4461359	0	3 AUGUGs Network	Seabird Glider Payload CTD(GPCTD)	1000 m	Structures of ME
3	AUGUG	Jul. 14-AUGUG. 13, 2017 30 days	30462998	3(Syntax Test)	10 AUGUGs, Network	Seabird Glider Payload CTD/GPCTD; Amended oxygen optode probes and WETLabs-fluorescent probes-#	300 m (3) 1000 m (7)	ME response to TC
4	AUGUG	Apr. 22-May 23, 2018; 31 days	239	0	1 AUGUG, Virtual mooring	Seabird Glider Payload CTD(GPCTD)	1000 m	Structures of ME
5	AUGUG	Jul. 13- Sept. 30, 2019; 77 days	458493707	3(Syntax Test)	50-17 AUGUGs, Network	Seabird Glider Payload CTD(GPCTD) *	300-400 (4) 1000 m (1742) 4500-4000 (4)	Slope intrusion of ME
6	AUV	Sept. 18- Oct. 23, 2019; 35 days	442131	5(Gross Range Test)	1 AUV	SBE37 CTD; DVL++	300 m	Evolution of ME
7	AUGUG	Jun. 26- AUGUG. 27, 2020; 60 days	35453365	14(Location Test& Syntax Test)	12 AUGUGs	Seabird Glider Payload CTD(GPCTD)	1000 m	Slope current
8	AUGUG	Jul. 26- AUGUG. 8, 2021; 13 days	467307	8(Syntax Test); 152(Gross Range Test);	2 AUGUGs	RBR legato CTD	300 m (1) 1000 m (1)	Edge of ME
9	AUGUG	AUGUG. 7- AUGUG. 27, 2021; 20 days	219215	4(Gross Range Test);	2 AUGUGs	Seabird Glider Payload CTD(GPCTD)	1000 m	Edge of ME
10	AUV	May 9- Jul. 29, 2021; 80 days	469167	2(Gross Range Test);	1 AUV	SBE37 CTD	300 m	Evolution of ME
11	AUGUG	Jun. 23- Jul. 6, 2022; 13 days	217	0	2 AUGUGs	Seabird Glider Payload CTD(GPCTD)	1000 m	Edge of ME
Total	/	463 days	2449812932	191	83-50 AUGUGs, 2 AUVs	/	/	Structures and evolution of ME

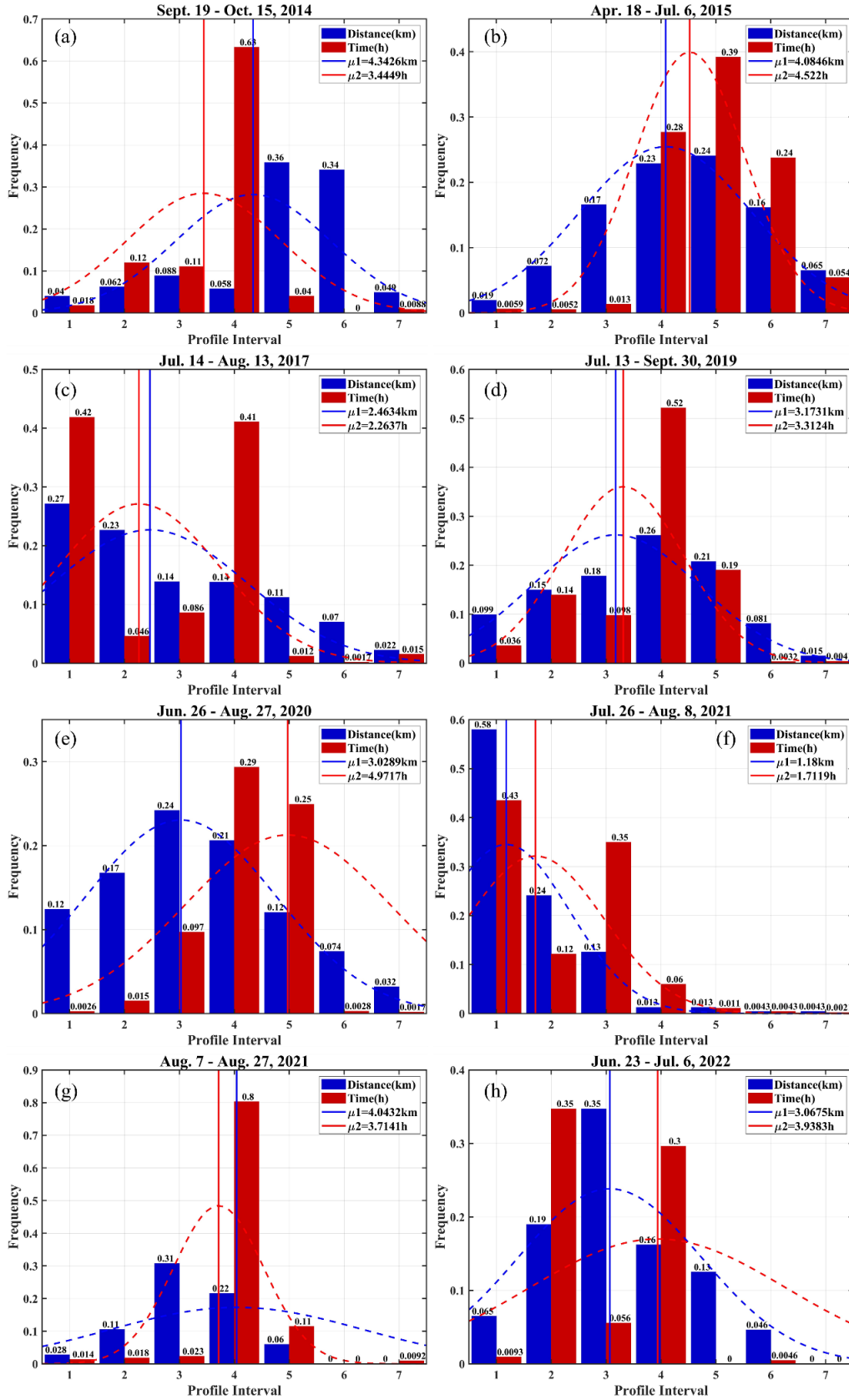


126
127
128
129
130
131
132
133
134

Figure 1. Underwater glider (UG) and autonomous underwater vehicle (AUV) observation sites. (A) observation area for subplots (a)-(e); (B) area for subplots (f)-(j). The grey lines in (A) and (B) are the water depth. (a)-(j) Observation stations (pink dots) with sea level anomaly (SLA, shading colors). The observation times are (a) September, 2014; (b) April, 2015; (c) July, 2017; (d) April, 2018; (e) July, 2019; (f) September, 2019; (g) June, 2020; (h) May, 2021; (i) July, 2021; (j) August, 2021; and (k) June, 2022.

2.2 Intercomparison of AUGUGs / AUVs resolution

The AUGUGs and AUVs positions with the mean sea level anomalies (SLAs) during experiment time were shown in Figure 1. Note that all the AUGUGs and AUVs crossed MEs with positive/negative SLAs. The spatial and temporal resolutions of samples were presented in Figure 2. The dominant spatial resolution (blue bars) was 4-7 km in 2014, 2015, and 2019, while it was less than 3 km in other years. In 2017 (Figure 2c), July 2021 (Figure 2f) and 2022 (Figure 2h), the temporal resolution of AUGUGs achieved 1-2 hours, while it was 4-7 hours in other experiments. It indicates that all of the experiments could resolve the MEs (spatial scale of 50-300 km), and 40% of them could be used to resolve submesoscale processes (spatial scale of <3 km).



145

146

147

148

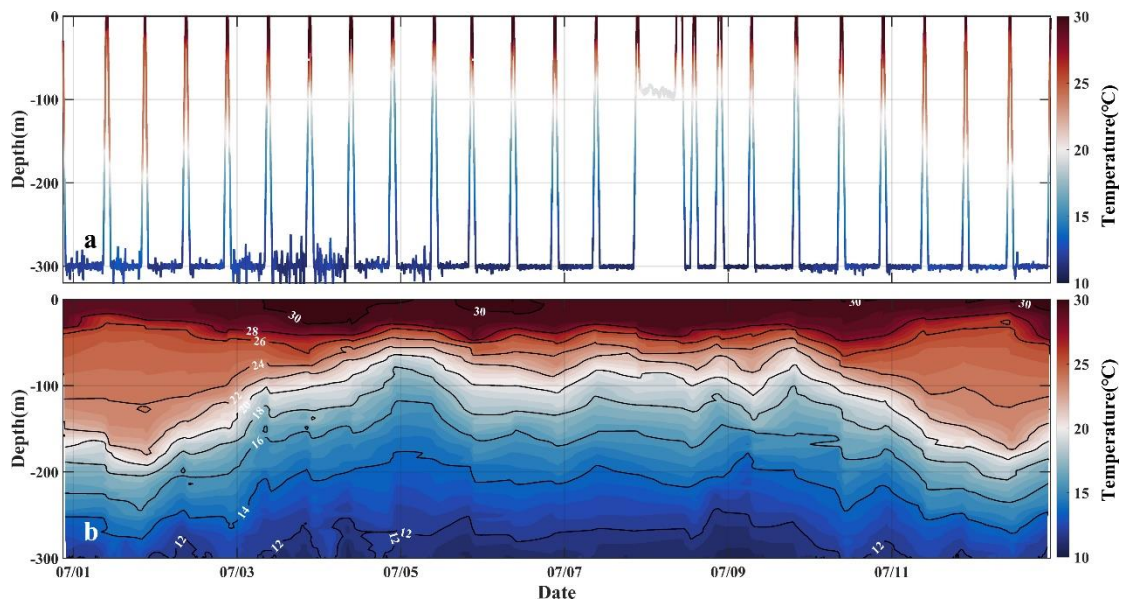
Figure 2. Frequency of spatial (blue bar) and temporal (red bar) sample interval. The red and blue bars (dashed red and blue lines) denote probabilities of spatial and time interval (the normal distributions of spatial and time intervals), respectively.

149 **3 Data Quality Control Method**

150 Before investigating the three-dimensional structures of MEs, we did quality control
151 for the **AUGUGs** and AUVs.

152 **3.1 Quality control for **AUGUG** data**

153 Two products of Chinese **AUGUGs** named “Sea-wing” and “Petrel” were used in
154 this study. The communication and navigation subsystem contain iridium satellite
155 communication devices, wireless communication devices, a precision navigation
156 attitude sensor, a Global Positioning System (GPS) device, a pressure meter, and
157 obstacle avoidance sonar. A conductivity-temperature-depth (CTD) sensor with ~6 s
158 sampling resolutions has been installed on the two **AUGUG** products.



159
160 Figure 3. Illustration of (a) original, and (b) interpolated data after quality control. The AUV

161 duration is in July 2021. [AUV: autonomous unmanned vehicle.](#)

162 Before investigating oceanic phenomena, we did data quality control [following](#)
163 [standard of integrated ocean observing system \(IOOS\).](#) The quality control for UG
164 <https://repository.oceanbestpractices.org/handle/11329/289?show=full> includes [9](#)
165 [steps: \(1\) Timing/Gap Test: Test determines that the profile has been received within](#)
166 [the expected time window and has the correct time stamp;](#) (2) Syntax Test: Ensures the
167 structural integrity of data messages; (3) Location Test: Test if the reported physical
168 [location \(latitude and longitude\) is within the reasonable range determined by the](#)

operator;(4) Gross Range Test: Ensure that the data points do not exceed the minimum/maximum output range of the sensor; (5) Pressure Test: Test if the pressure records increase monotonically with depth, sorted the vertical depth values and removed any duplicate depth values; (6) Climatology Test: Test if the data points are within the seasonal expectation range; (7) Spike Test: Test if the data points exceed the selected threshold compared to adjacent data points, excluded the data with temperature/salinity larger than 35 °C/35 psu; (8) Rate of Change Test: Test if the rate of change in the time series exceeds the threshold determined by the operator; (9) Flat Line Test: Test for continuously repeated observations of the same value, which may be the result of sensor or data collection platform failure. After that a natural neighbored interpolation is utilized to the temperature and salinity to 1-m vertical resolution data.

We have validated the AUGUG observed temperature and salinity profiles with ship observed data during July, 2019 (black star in Figure 1e; Figure 4). The mean bias of temperature is 0.05 °C , and that of salinity is 0.01 psu. The vertical temperature/salinity profiles of ship and AUGUG installed CTD are consistent, supporting that the data are credible.

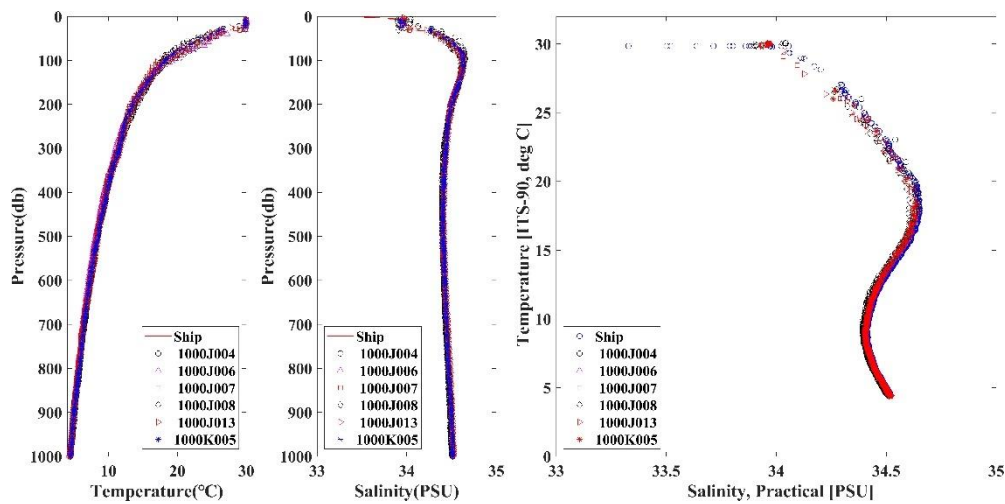


Figure 4. Comparison of (a) temperature, (b) salinity, and (c) temperature-salinity scatter plots between ship installed CTD and AUV installed CTD at station (112.0661°E, 17.7778°N). Red line in (a) and (b) is the ship measured values. Dot, green triangle, red square, diamond, red triangle, and blue star are for UGs named 1000J004, 1000J006, 1000J007, 1000J008, 1000J013 and 1000K005, respectively. Different symbols are the different AUG.

3.2 Quality control for AUV data

193 Both CTD and GPS instrument were installed on the “Sea-Whale 2000” AUV. This
 194 AUV was designed by Institute of Shenyang Automation, Chinese Academy of
 195 Sciences. It could operate in two modes, a “sawtooth-like” mode and a “cruise” mode
 196 at a depth of 300 m (Huang et al., 2019).

197 In the “sawtooth-like” mode, the data quality control procedures are the same as
 198 those for **AUGUGs**. Figures 3 and 4 show the AUV observed temperature after data-
 199 quality. In “cruise” mode, the AUV navigates at the depth of around 300 m. Following
 200 Qiu et al (2020), we firstly transformed the temperature and salinity at depth z to those
 201 at 300 m using a linear regression method ($T' = 0.008z' + 0.017$; $S' = -0.0002z' +$
 202 0.0006),

$$203 \quad T' = T_z - T_{mean}, \quad (1a)$$

$$204 \quad S' = S_z - S_{mean}, \quad (1b)$$

205 where T_{mean} is averaged using a 10-point smooth average, which could maintain the
 206 spatial variations from 20 to 30 km. Depth anomaly is defined as the measured depth
 207 minus 300 m, $z' = z - 300$, and the temperature and salinity anomalies as T' and S' ,
 208 respectively. We compared this method with the potential temperature algorithm, and
 209 the temperatures obtained at 300 m were highly consistent.

210 **3.3 Density derived from temperature and salinity**

211 The value of seawater density (ρ , in kg/m^3) can be calculated based on temperature
 212 (T in $^\circ\text{C}$), salinity (S in psu), and pressure (P in dbar). The UNESCO formula provides
 213 a simplified approach to estimate seawater density as follows:

$$214 \quad \rho(S, T, P) = \frac{\rho_0(S, T)}{1 - \frac{P}{K(S, T, P)}} \quad (2a)$$

$$215 \quad \rho_0(S, T) = \rho_{sw}(T) + (b_0 + b_1 T_{68} + b_2 T_{68}^2 + b_3 T_{68}^3 + b_4 T_{68}^4)S$$

$$+ (c_0 + c_1 T_{68} + c_2 T_{68}^2)S\sqrt{S} + d_0 S^2 \quad (2b)$$

$$216 \quad \rho_{sw}(T) = a_0 + a_1 T_{68} + a_2 T_{68}^2 + a_3 T_{68}^3 + a_4 T_{68}^4 + a_5 T_{68}^5 \quad (2c)$$

$$217 \quad T_{68} = T \times 1.00024 \quad (2d)$$

218 where $K(S, T, P)$ is secant bulk modulus, a_0 and others are coefficients. This formula
 219 accounts for the haline and thermal contraction of seawater. The detailed method is

220 [related to https://unesdoc.unesco.org/ark:/48223/pf0000188170.](https://unesdoc.unesco.org/ark:/48223/pf0000188170)

221

222 **4. Data Application**

223 **4.1 Intra-thermocline (Subsurface) MEs observed by **AUGUG**s and AUVs**

224 Cross-eddy tracks of **AUGUG** or AUV could observe both the warm core and cold
225 cores (Figure 4). In April 2015, one **AUGUG** crossed a warm eddy, and observed a
226 subsurface warm core (Figure 1b & Figure 5a). The warm core ranges from 50-500 m
227 depth with radius about 100 km, which is termed as intra-thermocline anticyclone and
228 has been reported in Shu et al (2016). Qiu et al (2019) utilized the same experimental
229 dataset to investigate the asymmetry structures of this intra-thermocline eddies,
230 suggesting that the centrifugal force should be taken into account when revealing the
231 velocity of MEs, i.e. gradient wind theory. This gradient wind theory has been cited in
232 a deriving global cyclogeostrophic currents data (Cao et al. 2023). In June 2020
233 (Figures 1g & 5d-f), one **AUGUG** captured a subsurface cold eddy with a negative
234 temperature and positive salinity core, which is the value minus the zonal mean value.
235 And the highly dense core ranged from surface to 500 m depth. Above all, single
236 **AUGUG**/AUV could capture both the surface and the intra-thermocline eddy's position,
237 range and strength.

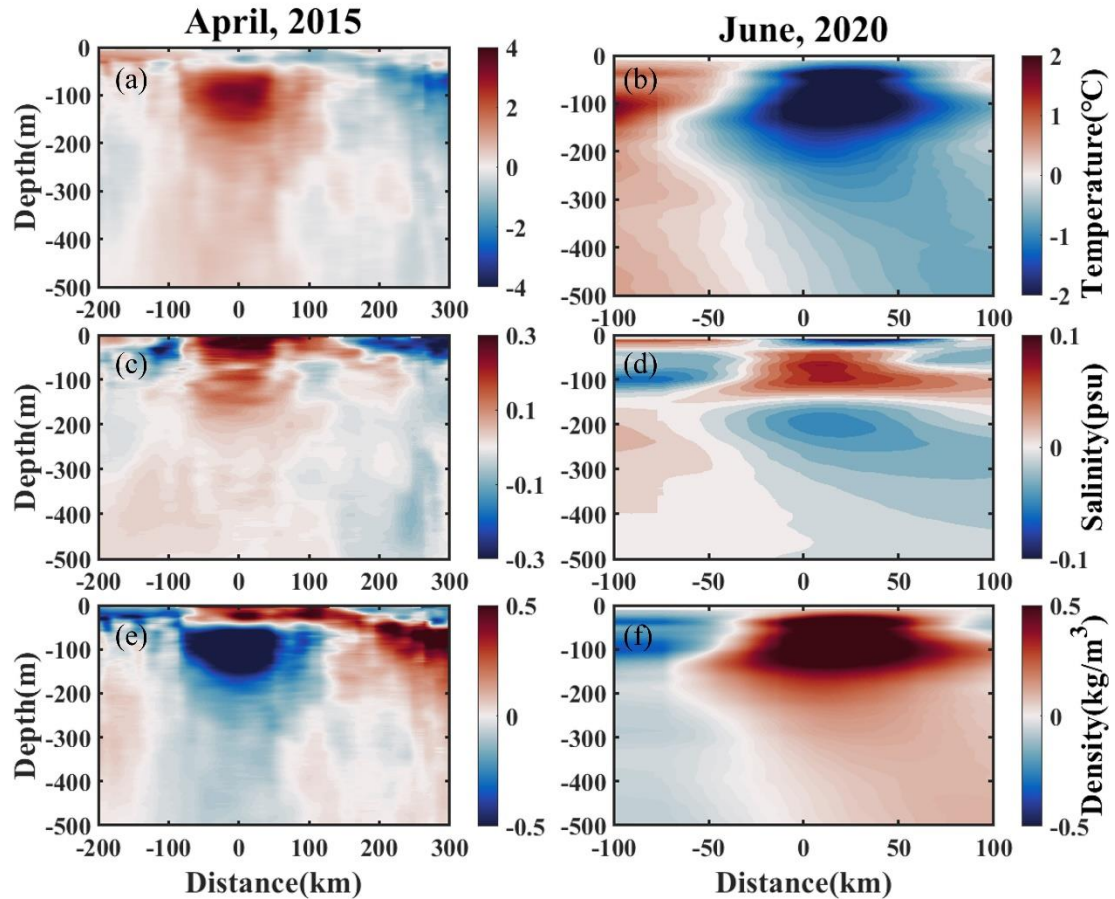
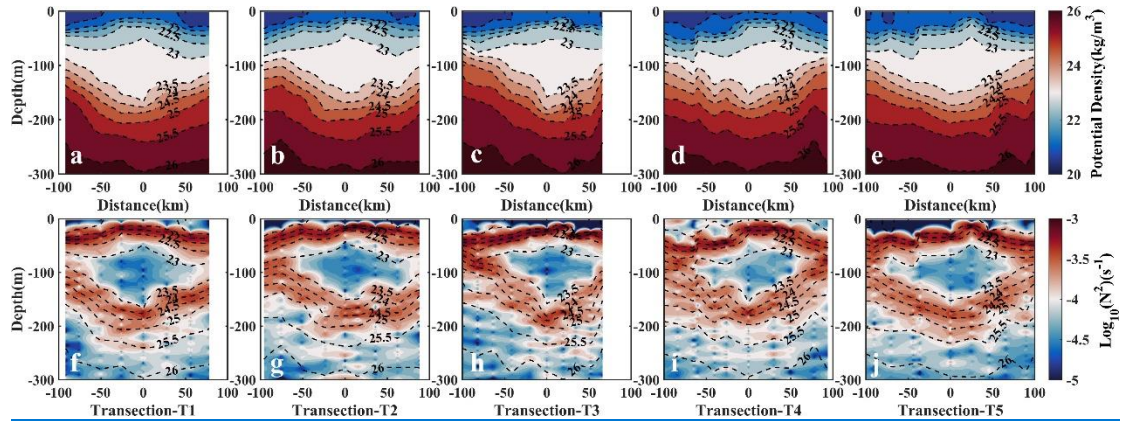


Figure 5. Contour of (a) and (b) temperature anomaly (c) and (d) salinity anomaly, (e) and (f) density anomaly in April, 2015(left panels) and June, 2020(right panels).

AUGUG/AUV could track the development of intra-thermocline MEs. During developing stage, MEs can easily deform and may cause cross-slope transports at the continental slope (Wang et al., 2018; Su et al., 2020; Qiu et al., 2022), and produce submesoscale process (Dong et al., 2018; Yang et al., 2019). To observe the development of ME, “Sea-Whale 2000” AUV have traversed an anticyclonic ME using 5 repeated rectangular tracks from May to July 2021(Figure 1h). This experiment was supported by National Key R&D Program.

An anti-cyclonic eddy with low Brunt-Väisälä frequency squared value ($N^2 = \frac{1}{\rho} \frac{d\rho}{dz} < 10^{-4} \text{ s}^{-1}$), located in the subsurface layer from 50-200 m depth, and existed as an intra-thermocline anticyclonic eddy (Figure 6). The repeated cruise of AUV was separated to five stages, termed as T1(June 8-11), T2 (June 19-23), T3 (June 29- July 4), T4 (July 10- 15), and T5 (July 21-26). Taking 22.5 kg/m^3 and 23.5 kg/m^3 as the

254 upper and lower boundary of the intra-thermocline ME, we calculated the area and the
 255 mean temperature within the mesoscale eddy. The area and mean temperature decreased
 256 from T1-T3, and then increased from T4-T5, indicating the intra-thermocline
 257 anticyclonic eddy weakened from T1-T3 and strengthened from T4-T5. This
 258 development has been described in detail by Qiao et al (2023), who found the eddy
 259 moved eastward during T1-T3 and got stuck during T4-T5.



260 Figure 6. The profiles of density (upper panel) and Brunt frequency (lower panel) during (a,f)T1,
 261 (b,g)T2, (c,h)T3, (d, i)T4, (e, j)T5 period, which was 06/08-06/11,06/19-06/23,06/29-07/04,07/10-
 262 07/15,07/21-07/26, respectively.
 263

265 4.2 Vertical Tilt of MEs at different life-stages observed by **AUGUGs**

266 Several systematic **AUGUG** networks were conducted in 2015, 2017, 2019, and
 267 2020. A whole life cycle of ME usually experiences birth, developing, mature and
 268 dissipate stages (Zhang and Qiu, 2018; Yang et al., 2019), and the eddy's age has
 269 suggested to influence on the kinetic energy of ME. Luzon strait is an eddy birth zone,
 270 where Kuroshio branch intrudes the SCS (Chen et al., 2011; Su et al., 2020). And then,
 271 most of the eddies move westward to the continental shelf zone under the modulation
 272 of Rossby wave, finally dissipate in Dongsha Islands, Xisha Islands or merged with
 273 other eddies (Yang et al., 2019; Su et al., 2020; Qiu et al., 2022).

274 The systematic **AUGUG** experiments provide us probability in capturing the
 275 different vertical structures of MEs at different life stages. After data quality, we firstly
 276 mapped the temperature and salinity data onto $1 \text{ km} \times 1 \text{ km} \times 1 \text{ m}$ grid, and then

277 calculated the water density, ρ . The ME follows geostrophic balance, that is, the
278 geostrophic velocity could be derived under the force balances between pressure
279 gradient and Coriolis force. Finally, we derived the geostrophic velocity, v_g , by using
280 thermal-wind relationships,

$$281 \quad v_g(x, y, z) = v_0 - \frac{g}{f\rho_0} \int_{z_0}^z \left(\frac{\partial \rho(x, y, z)}{\partial x} + \frac{\partial \rho(x, y, z)}{\partial y} \right) dz, \quad (3)$$

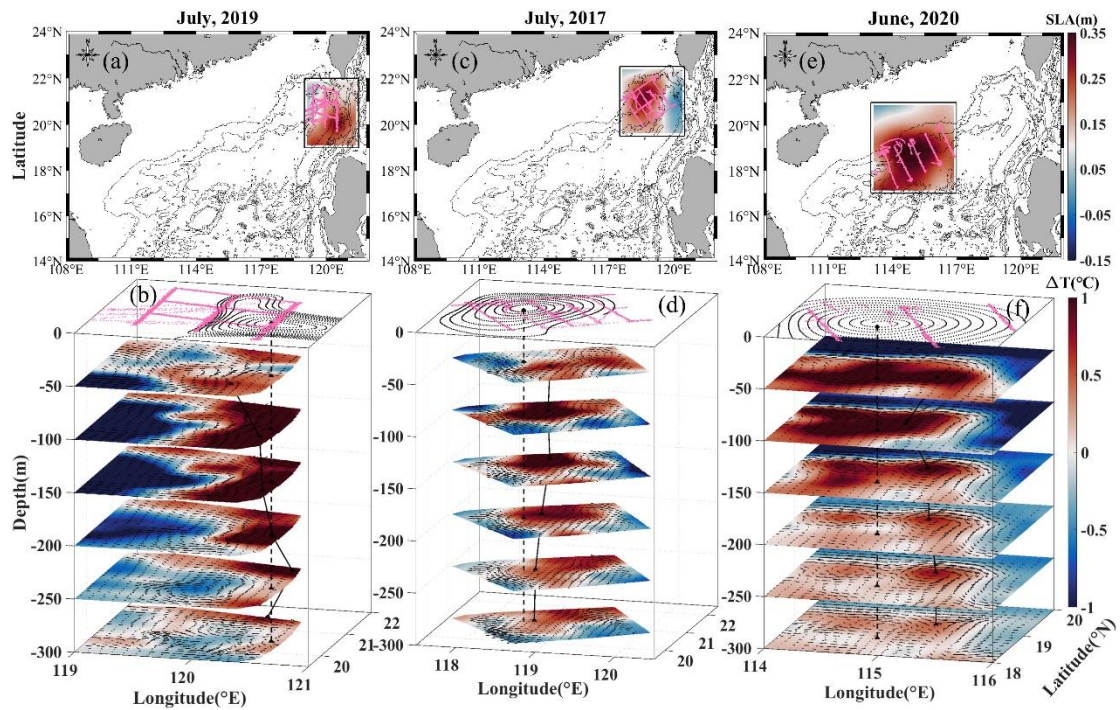
282 where ρ_0 is the referenced water density, f is the Coriolis frequency, v_0 is the
283 referenced geostrophic velocity at depth 1000 m and assumed to be 0.

284 Figure 7a-b depicts the three-dimensional temperature and velocity structures of a
285 ME (120 °E) at birth stage, as observed by 12 AUGUGs in July 2019 (Figure 1e&6a-
286 b). A warm core was located at subsurface layer and the eddy center exhibited a
287 northeastward vertical tilt (solid black line). In July 2017 (Figures 1c & 6c-d), 10
288 AUGUGs were deployed westward to the Luzon Strait (119 °E). This eddy was in its
289 developing phase and possessed a significant eastward vertical tilt from deep up to
290 surface, reaching depths deeper than 500 m. The eastward vertical tilt is suggested to
291 have been induced by the background current, westward propagation of Rossby Waves
292 (e.g., Qiu et al., 2015; Zhang et al., 2016; Li et al., 2019), and advection background
293 temperature gradient (e.g., Bonnici& Billant, 2020; Gaube et al., 2015; Li, Wang, et al.,
294 2020). Throughout this experiment, the AUGUGs encountered the tropical storm
295 “Haitang”, results in that the ME underwent horizontal deformation, giving rise to
296 submesoscale processes (Yi et al., 2022; Yi et al., 2024).

297 In June 2020, 6 AUGUGs were deployed across another warm ME in the shelf
298 region (Figures 1g and 6e-h). The eddy was under dissipating stage due to the steep
299 topography, displaying a significant southwestward tilt from a depth of 500 m to surface
300 (Figure 7e-7f). This kind of southwestward vertical tilt was revealed by potential
301 vorticity in a numerical model (Qiu et al., 2022), which was attributed to shallower
302 water depth to the west of mesoscale eddies, and caused asymmetries of the velocities
303 within the MEs. Qiao et al (2023) also captured an eastward movement of a ME by
304 using AUV observations in June 2021(Figure 1h). Based on tensor decomposition of
305 barotropic instability energy, they suggested wave-current interaction played the most

306 important role in the development and propagation of this eddy.

307



308

309 Figure 7. Eddy structures during periods of (a-b) eddy burst/birth, (c-d) westward movement, and
310 (e-f) dissipation along slope movements. Sea level anomaly (SLA) and AUGUGs' positions are
311 superimposed in upper panels (a, c, e), isobaths are represented by solid lines. The AUGUG
312 observed temperature and derived geostrophic velocities are in the 3D plots (b, d, f). Pink lines are
313 the tracks of AUGUGs. Dashed lines denote the centers of mesoscale eddies from SLA fields, and
314 solid dot lines are the centers from warm cores. UG: Underwater Glider.

315

316 **4.3 Submesoscale instabilities at the edge of MEs observed by AUGUGs**

317 Fine structures, i.e., submesoscale process, usually occurs within MEs, either at the
318 eddy edge (front; filament) or entrained in the eddy center, in terms of spiral structures
319 or “eye-cat” structures (Zhang and Qiu, 2018; Ni et al., 2021; Hu et al., 2023; Qiu et
320 al., 2024). They could cascade kinetic energy downward to turbulent scale via
321 symmetric or centrifugal instabilities, and also induce kinetic energy inverse cascade to
322 MEs via mixed layer baroclinic instabilities (i.e., Fox-Kemper et al., 2008; McWilliams,
323 2016). However, the submesoscale processes within MEs are difficult to be observed
324 by Argo with 10-day's temporal resolution. Tang et al. (2022) attempted to observe
325 submesoscale fronts using NAVIS float, and found that mixed-layer baroclinic

326 instability dominated this frontogenesis. Qiu et al. (2019) and Shang et al (2023) have
 327 captured the submesoscale front at the eddy's edge by using a "virtual mooring"
 328 **AUGUG** observation. As passively driven by flow, NAVIS can only observe
 329 submesoscale process in an approximate Lagrangian fashion, whereas **AUGUGs**
 330 traversing a front could provide us both the cross-front and along-front information,
 331 depending on our observational scheme.

332 In our datasets, 40% of **AUGUG** observations have high spatiotemporal resolutions
 333 (<3 km, <4 h; Figure 2), which are fine enough to capture the submesoscale processes
 334 positively. Here, we present two examples of submesoscale instabilities at the edge of
 335 MEs to show the advantages of **AUGUG** observations.

336 As shown in Figure 8a, 4 diving **AUGUGs** were deployed at the eddy's edge (front)
 337 in 2017. 3 **AUGUGs** cross the front and 1 **AUGUG** tracks along the front. All of them
 338 successfully observed the submesoscale instabilities. Following Thomas *et al* (2013),
 339 the converted angle of the Richardson number, ϕ_{Ri} , can also be used to determine the
 340 nature of the instability:

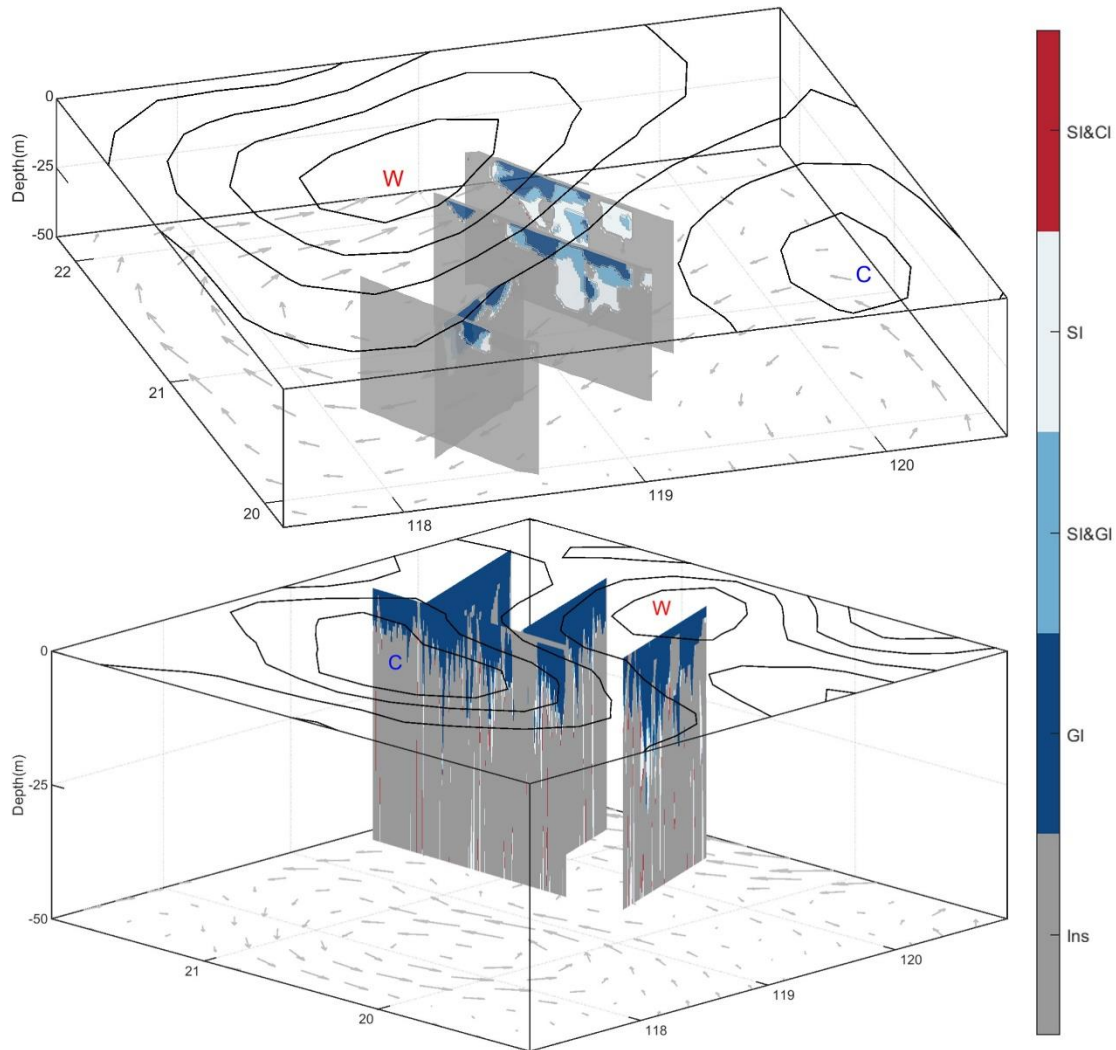
$$341 \quad \phi_{Ri} = \tan^{-1} \left(-\frac{1}{Ri} \right) = \tan^{-1} \left(\frac{|\vec{v} \cdot \vec{b}|^2}{N^2 \cdot f^2} \right), \quad (3a)$$

$$342 \quad Ri \approx Ri_g = \frac{N^2}{\left(\frac{\partial \vec{v}_g}{\partial z} \right)^2} = \frac{N^2 \cdot f^2}{|\vec{v} \cdot \vec{b}|^2} < \frac{f}{\zeta_g}, \text{ and } f \cdot \zeta_g > 0. \quad (3b)$$

343 where f is the Coriolis parameter, and \vec{v}_g is the geostrophic velocity. $b = -g\rho/\rho_0$, is
 344 the buoyancy flux, g is the gravitational acceleration, and ρ is the seawater density, and
 345 ρ_0 is the reference density. $N^2 = \partial b/\partial z$ is the vertical buoyancy frequency. $\zeta_g =$
 346 $curl(\vec{v}_g)$ is the vertical relative vorticity. ϕ_{Ri} can be used to judge when instability
 347 occurs. For anticyclonic eddies, inertial instability or symmetric instability occurs when
 348 $-45^\circ < \phi_{Ri} < \phi_c$; symmetric instability occurs when $-90^\circ < \phi_{Ri} < -45^\circ$;
 349 symmetry instability or gravitational instability occurs when $-135^\circ < \phi_{Ri} < -90^\circ$;
 350 and gravitational instability occurs when $-180^\circ < \phi_{Ri} < -135^\circ$.

351 Figure 8a shows that **AUGUGs** observed several types of submesoscale instabilities,
 352 in terms of gravity instability, symmetric instability and mixed instabilities from
 353 symmetric and centrifugal instabilities at the anticyclonic eddy's edge. Figure 8b shows

354 submesoscale instabilities in 2019. In this case, gravity instability dominates the upper
355 mixed layer. Symmetric and centrifugal instabilities are not significant. These two cases
356 provide us enough information to detect frontal genesis processes in Euler field, while
357 Navis or Argos provide frontal information in Lagrange view.



358

359 Figure 8. Analyzed submesoscale instabilities at the edge of mesoscale eddies. (a) in 2017, and (b)
360 in 2019. SI: symmetric instability; CI: centrifugal instability; GI: gravity instability. W:
361 anticyclonic eddy; C: cyclonic eddy. Isolines are the sea level anomaly.

362

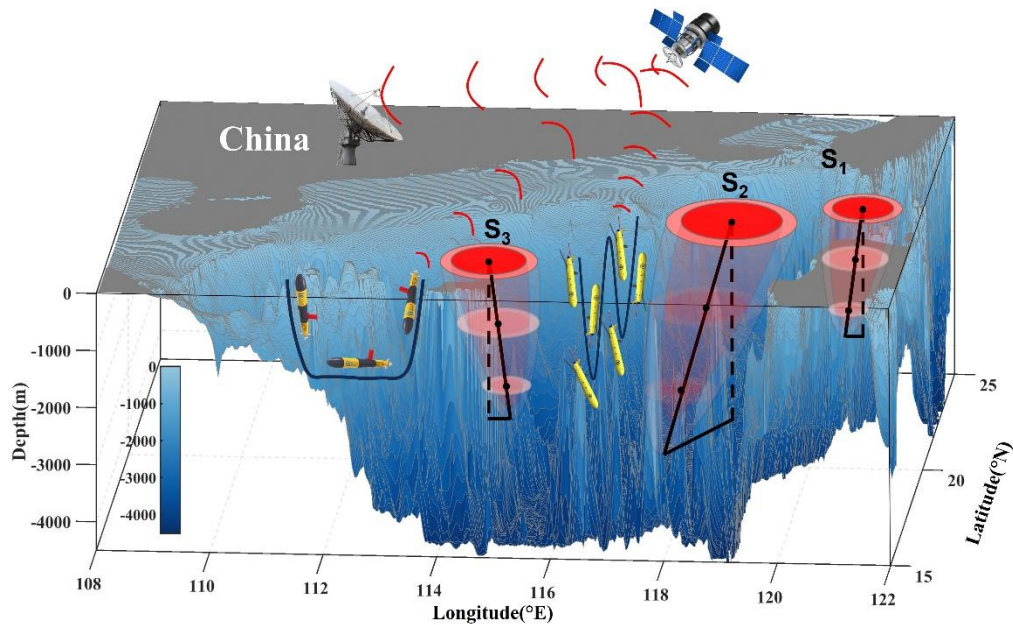
363 5. Data availability

364 The dataset of AUV and [AUGUG](#) used in this manuscript was deposited in Science
365 Data Bank, whose DOI is <https://doi.org/10.57760/sciencedb.11996> (Qiu et al., 2024b).

366

367

6. Conclusions and Potential Future Plan



368

369 Figure 9. Scheme of AUGUGs observed mesoscale eddies at different life stages in the
 370 northern SCS. S1: birth stage; S2: developing/mature stage; S3: dissipating stage. UG: Underwater
 371 Glider; SCS: South China Sea.

372

373 Based on 9-year AUVs and AUGUGs observations in SCS, we obtained high-
 374 resolution temperature and salinity profiles datasets in SCS. The dataset provides 24498
 375 profiles and covers 463 days' experiments, including 11 experiments from 50 AUGUGs
 376 and 2 AUVs. To our knowledge, the 9-year dataset is enough in detecting the horizontal
 377 asymmetry, vertical tilt, temporal evolution, life cycle of MEs (Figure 9), and the
 378 associated submesoscale processes. The dataset supports us to investigate the
 379 subsurface MEs, revealing eddy-current and eddy-topography interactions successfully.
 380 However, to understand the feedback of MEs to the variability of larger scale current,
 381 i.e. western boundary current, routine AUGUGs and AUVs observations are needed in
 382 future.

383 Besides tracking MEs, AUGUGs and AUVs have been proved to positively capture
 384 more smaller scale oceanic process, such as internal tide (Gao et al., 2024), turbulences
 385 by using turbulent parameterization schemes (Qi et al, 2020). And AUGUGs/AUV
 386 installed with more sensors could also provide us geochemical parameters (e.g., Yi et

387 al., 2022), presenting the potential ability in improving the forecast accuracy in physical
388 and biogeochemical numerical model. More projects gathering AUVs network are
389 ongoing and will be promoted in future.

390 During the mission, we met some challenges: (1) under strong background current,
391 UGs and AUVs get disturbed and cannot follow the customized routes; (2) Under bad
392 weather, the it's difficult for piloting team to deploy and recovery UGs and AUVs; (3)
393 data receiving capacity depends on the satellite transmission capacity. If both the bio-
394 chemistry and CTD data are included, the data resolution have to be lowered. These
395 challenges require piloting team and oceanographers to work together.

396

397 **Author contributions**

398 Conceptualization: DX,~~JC~~; data curation: CH, ZY, ~~HB~~, ZH, ~~HB~~, JW, ~~YQ~~; formal
399 analysis: CH, ZY; funding acquisition: CH, DX,~~JC~~; investigation: CH, DX,~~JC~~;
400 methodology: CH, DX,~~JC~~; project administration: CH, DX,~~JC~~; software: CH, DX;
401 supervision: CH, DX; validation: XM, DX, ~~WB~~; writing: CH, XM. All the authors have
402 read and agreed to the published version of the manuscript.

403 **Financial support**

404 This study was supported by the National Natural Science Foundation of China
405 (Grant No. 42376011; 41976002), National Key R&D Plan Program
406 (No.2017YFC0305804).

407 **Competing interests**

408 The contact author has declared that none of the authors has any competing
409 interests.

410 **Acknowledgements**

411 We acknowledge all the colleagues and project members who have contributed to
412 the design of ~~AUGUG~~s and AUVs, the sea experiments and data processing in the past.
413 Many scientists and engineers have participated in active surveys and mappings. Their
414 work provided basic high-quality materials.

415 **Disclaimer**

416 Publisher's note: Copernicus Publications remains neutral with regard to
417 jurisdictional claims made in the text, published maps, institutional affiliations, or any
418 other geographical representation in this paper. While Copernicus Publications makes
419 every effort to include appropriate place names, the final responsibility lies with the
420 authors.
421
422

423

References:

- 424 [Bachmayer, R., Leonard, N. E., Graver, J., Fiorelli, E., Bhatta, P. and Paley, D. Underwater glider:](#)
425 [Recent developments and future applications, *Proceedings of the 2004 International*](#)
426 [Symposium on Underwater Technology, 2004, 195~200.](#)
427 [https://doi.org/10.1109/UT.2004.1405540.](https://doi.org/10.1109/UT.2004.1405540)
- 428 [Caffaz, A., Caiti, A., Casalino, G. and Turetta, A. The hybrid glider/AUV folaga, *IEEE Robotics and*](#)
429 [Automation Society, 2010, 17\(1\), 31~44. https://doi.org/10.1109/MRA.2010.935791.](#)
- 430 Cao, Y., Dong, C., Stegner, A., Bethel, B. J., Li, C., Dong, J., et al. (2023). Global sea surface
431 cyclogeostrophic currents derived from satellite altimetry data. *Journal of Geophysical*
432 *Research: Oceans*, 128, e2022JC019357. <https://doi.org/10.1029/2022JC019357>
- 433 Chen, G., Hou, Y., Chu, X. Mesoscale eddies in the South China Sea: Mean properties,
434 spatiotemporal variability, and impact on thermohaline structure. *Journal of Geophysical*
435 *Research-Oceans*, 2011, 116, C06018. <https://doi.org/10.1029/2010JC006716>
- 436 Chelton, D., Schlax, M., Samelson, R., de Szoeke, R. Global observations of large oceanic eddies.
437 *Geophysical Research Letters*, 2007, 34(15), L15606. <https://doi.org/10.1029/2007GL030812>
- 438 Chelton, D., Schlax, M., Samelson, R. Global observations of nonlinear mesoscale eddies. *Progress*
439 *in Oceanography*, 2011, 91 (2): 167–216, [doi:10.1016/j.pocean.2011.01.002](https://doi.org/10.1016/j.pocean.2011.01.002).
- 440 Chu, P., Chen, Y., Lu, S. Wind-driven South China Sea deep basin warm-core/cool-core eddies.
441 *Journal of Oceanography*, 1998, 54(4), 347-360. doi: 10.1007/bf02742619.
- 442 Chu, P., Fan, C. Optimal linear fitting for objective determination of ocean mixed layer depth from
443 glider profiles. *Journal of Atmospheric and Oceanic Technology*, 2010, 27, 1893–1898.
- 444 Dale, W. Winds and drift currents in the South China Sea. *Malayan Journal of Tropical Geography*,
445 1956, 8, 1-31.
- 446 Dong, C., McWilliams, J., C., Liu, Y., Chen D. Global heat and salt transports by eddy movement.
447 *Nature Communications*, 2014, 5(2), 3294.
- 448 Dong, J., Zhong, Y. The spatiotemporal features of submesoscale processes in the northeastern
449 South China Sea. *Acta Oceanology Sinica*, 2018, 37(11), 8-18. [https://doi.org/10.1007/s13131-](https://doi.org/10.1007/s13131-018-1277-2)
450 [018-1277-2.](https://doi.org/10.1007/s13131-018-1277-2)
- 451 [Eriksen, C. C., Osse, T. J., Light, R. D., Wen, T., Lehmann, T. W., Sabin, P. L., Ballard, J. W. and](#)
452 [Chiodi, A. M. Seaglider: A long range autonomous underwater vehicle for oceanographic](#)
453 [research, *IEEE Journal of Oceanic Engineering*, 2001, 26\(4\), 424~436. https://doi.org/](#)
454 [10.1109/48.972073.](https://doi.org/10.1109/48.972073)
- 455 Fang, W., Fang, G., Shi, P., Huang, Q., Xie, Q. Seasonal structures of upper layer circulation in the
456 southern South China Sea from in situ observations. *Journal of Geophysical Research: Oceans*,
457 2002, 107(C11), 23-1-23-2. doi: 10.1029/2002JC001343.
- 458 Fox-Kemper, B., Ferrari, R., Hallberg, R. Parameterization of mixed layer eddies. Part I: Theory
459 and diagnosis. *Journal of Physical Oceanography*, 2008, 38(6), 1145-1165.
460 <https://doi.org/10.1175/2007JPO3792.1>
- 461 Gao, Z., Chen, Z., Huang, X., Yang, H., Wang, Y., Ma, W., & Luo, C. (2024). Estimating the energy
462 flux of internal tides in the northern South China Sea using underwater gliders. *Journal of*
463 *Geophysical Research: Oceans*, 129, e2023JC020385. <https://doi.org/10.1029/2023JC020385>
- 464 He, Q., Zhan, H., Cai, S., He, Y., Huang, G., Zhan, W. A new assessment of mesoscale eddies in the
465 South China Sea: surface features, three-dimensional structures, and thermohaline transports.
466 *Journal of Geophysical Research: Oceans*, 2018, 123(7), 4906-4929.

467 <https://doi.org/10.1029/2018JC014054>

468 He, Q., Zhan, H., Xu, J., Cai, S., Zhan, W., Zhou, L., Zha, G. Eddy-induced chlorophyll anomalies
469 in the western South China Sea. *Journal of Geophysical Research: Oceans*, 2019, 124,
470 <https://doi.org/10.1029/2019JC015371>.

471 He, Y., Xie, J., Cai, S. Interannual variability of winter eddy patterns in the eastern South China Sea.
472 *Geophysical Research Letters*, 2016, 43(10), 5185-5193. doi: 10.1002/2016GL068842.

473 [Hobson, B. W., Bellingham, J. G., Kieft, B., McEwen, R., Godin, M. and Zhang, Y. Tethys-class](#)
474 [long range AUVs - extending the endurance of propeller-driven cruising AUVs from days to](#)
475 [weeks. 2012 IEEE/OES Autonomous Underwater Vehicles \(AUV\), 2012, 1-8,](#)
476 <https://doi.org/10.1109/AUV.2012.6380735>.

477 Hu, Z., Lin, H., Liu Z., Cao Z., Zhang F., Jiang Z., Zhang Y., Zhou K., and Dai M. Observations of
478 a filamentous intrusion and vigorous submesoscale turbulence within a cyclonic mesoscale
479 eddy, *Journal of Physical Oceanography*, 2023, 53(6), 1615–1627.

480 Huang, Y., Qiao, J., Yu, J., Wang, Z., Xie, Z., Liu, K. Sea-Whale 2000: a long-range hybrid
481 autonomous underwater vehicle for ocean observations. *OCEANS 2019 - Marseille*, Marseille,
482 France, 2019, 1-6, doi: 10.1109/OCEANSE.2019.8867050.

483 Hwang, C., Chen, S. Circulations and eddies over the South China Sea derived from
484 TOPEX/Poseidon altimetry. *Journal of Geophysical Research: Oceans*, 2000, 105(C10),
485 23943-23965. doi: 10.1029/2000JC900092.

486 Li, H., Xu, F., Wang, G. Global mapping of mesoscale eddy vertical tilt. *Journal of Geophysical*
487 *Research: Oceans*, 2022, 127, e2022JC019131. <https://doi.org/10.1029/2022JC019131>

488 Li, L., Worth, D., Nowlin, J., Su, J. Anticyclonic rings from the Kuroshio in the South China Sea.
489 *Deep Sea Research Part I*, 1998, 45, 1469-1482. doi: 10.1016/s0967-0637(98)00026-0.

490 Lin, X., Dong, C., Chen, D., Liu, Y., Yang, J., Zou, B., Guan, Y. Three-dimensional properties of
491 mesoscale eddies in the South China Sea based on eddy-resolving model output. *Deep-Sea*
492 *Research Part I: Oceanographic Research Papers*, 2015, 99, 46-64.
493 <https://doi.org/10.1016/j.dsr.2015.01.007>

494 Lin, P., Wang, F., Chen, Y., & Tang, X. Temporal and spatial variation characteristics of eddies in
495 the South China Sea I: Statistical analyses. *Acta Oceanologica Sinica*, 2007, 29(3), 14-22.

496 McWilliams, J. Submesoscale currents in the ocean. *Proceedings of the Royal Society A*, 2016, 472,
497 20160117. <http://dx.doi.org/10.1098/rspa.2016.0117>

498 Morison, J., Andersen, R., Larson, N., D'Asaro, E., Boyd, T. The correction for thermal-lag effects
499 in Sea-Bird CTD data. *Journal of Atmospheric and Oceanic Technology*, 1994, 11, 1151–1164,
500 [https://doi.org/10.1175/1520-0426\(1994\)011,1151:TCFTLE.2.0.CO;2](https://doi.org/10.1175/1520-0426(1994)011<1151:TCFTLE.2.0.CO;2).

501 Morrow, R., Birol, F., Griffin, D., Sudre, J. Divergent pathways of cyclonic and anti-cyclonic ocean
502 eddies. *Geophysical Research Letters*, 2004, 31(24), L24311.
503 <https://doi.org/10.1029/2004gl020974>

504 Nan, F., He, Z., Zhou, H., Wang, D. Three long-lived anticyclonic eddies in the northern South
505 China Sea. *Journal of Geophysical Research: Oceans*, 2011, 116(5), C05002.
506 <https://doi.org/10.1029/2010JC006790>

507 Ni, Q., Zhai, X., Wilson, C., Chen, C., Chen, D. Submesoscale eddies in the South China Sea.
508 *Geophysical Research Letters*, 2021, 48, e2020GL091555.
509 <https://doi.org/10.1029/2020GL091555>

510 Oey, L. Eddy- and wind-forced shelf circulation. *Journal of Geophysical Research*, 1995, 100(C5),

511 8621–8637.<https://doi.org/10.1029/95JC00785>.

512 Okkonen, S., Weingartner, T., Danielson, S., Musgrave, D., Schmidt, G. M. Satellite and
513 hydrographic observations of eddy-induced shelf-slope exchange in the northwestern Gulf of
514 Alaska. *Journal of Geophysical Research*, 2003, 108(C2), 3033.
515 <https://doi.org/10.1029/2002JC001342>.

516 [Osse, T. J. and Eriksen, C. C. The deepglider: a full ocean depth glider for oceanographic research.](#)
517 [OCEANS 2007, 2007, 1–12. https://doi.org/10.1109/OCEANS.2007.4449125.](#)

518 Qi, Y., Shang, C., Mao, H., Qiu, C., Shang, X. Spatial structure of turbulent mixing of an
519 anticyclonic mesoscale eddy in the northern South China Sea. *Acta Oceanologica Sinica*, 2020,
520 39(11), 69-81. <https://doi.org/10.1007/s13131-020-1676-z>.

521 Qiao, J., Qiu, C., Wang, D., Huang, Y., Zhang, X., Huang, Y. Multi-stage Development within
522 Anisotropy Insight of an Anticyclone Eddy Northwestern South China Sea in 2021.
523 *Geophysical Research Letter*, 2023, doi:10.1029/2023GL104736

524 Qiu, C., Mao, H., Yu, J., Xie, Q., Wu, J., Lian, S., Liu, Q. Sea surface cooling in the Northern South
525 China Sea observed using Chinese Sea-wing Underwater Glider Measurements. *Deep Sea*
526 *Research Part I: Oceanographic Research Papers*, 2015, 105, 111-118.

527 Qiu, C., Mao, H., Liu, H., Xie, Q., Yu, J., Su, D., Ouyang, J., Lian, S. Deformation of a warm eddy
528 in the northern South China Sea. *Journal of Geophysical Research: Oceans*, 2019, 124, 5551-
529 5564. <https://doi.org/10.1029/2019JC015288>

530 Qiu, C., Mao, H., Wang, Y., Su, D., Lian, S. An irregularly shaped warm eddy observed by Chinese
531 underwater gliders. *Journal of Oceanography*, 2019, 75, 139-148.

532 Qiu, C., Liang, H., Huang, Y., Mao, H., Yu, J., Wang, D., Su, D. Development of double cyclonic
533 mesoscale eddies at around Xisha Islands observed by a ‘Sea-Whale 2000’ autonomous
534 underwater vehicle. *Applied Ocean Research*, 2020,
535 <https://doi.org/10.1016/j.apor.2020.102270>.

536 Qiu, C., Yi, Z., Su, D., Wu, Z., Liu, H., Lin, P., He, Y., Wang, D. Cross-slope heat and salt transport
537 induced by slope intrusion eddy’s horizontal asymmetry in the northern South China Sea.
538 *Journal of Geophysical Research: Oceans*, 2022, doi: 10.1029/2022JC018406.

539 Qiu, C., Yang, Z., Feng, M., Yang, J., Rippeth, T.P., Shang, X., Sun, Z., Jing, C., Wang,
540 D. Observational energy transfers of a spiral cold filament within an anticyclonic
541 eddy. *Progress in Oceanography*, 2024a, <https://doi.org/10.1016/j.pocean.2023.103187>.

542 Qiu, C., Du, Z., Yu, J., et al. **AUGUG** and AUV data used in research “A High Dense Temperature-
543 Salinity Dataset Observed by **AutomaticAutonomous** Underwater Vehicles toward Mesoscale
544 eddies’ Evolutions and Associated Submesoscale Processes in South China Sea” [DS/OL]. V2.
545 Science Data Bank, 2024b[2024-08-03]. <https://doi.org/10.57760/sciencedb.11996>. DOI:
546 10.57760/sciencedb.11996.

547 Rainville, L., Lee, C., Arulanathan, K., Jinadasa, S., Fernando, H., Priyadarshani, W., Wijesekera,
548 H. Water mass exchanges between the Bay of Bengal and Arabian Sea from multiyear sampling
549 with autonomous gliders. *Journal of Physical Oceanography*, 2022, 52, 2377–2396,
550 <https://doi.org/10.1175/JPO-D-21-0279.1>.

551 Shang, X., Shu, Y., Wang, D., Yu, J., Mao, H., Liu, D., Qiu, C., Tang, H. Submesoscale motions
552 driven by down-front wind around an anticyclonic eddy with a cold core. *Journal of*
553 *Geophysical Research: Oceans*, 2023, 128, e2022JC019173.
554 <https://doi.org/10.1029/2022JC019173>.

- 555 [Sherman, J., Davis, R. E., Owens, W. B. and Valdes, J., 2001. The autonomous underwater glider](#)
556 [“Spray”, IEEE J. Ocean Eng., 26\(4\): 437–446.](#)
- 557 Shu, Y., Xiu, P., Xue, H., Yao, J., Yu, J. (2016). Glider-observed anticyclonic eddy in northern South
558 China Sea. *Aquatic Ecosystem Health & Management*, 19(3), 233–241.
559 <https://doi.org/10.1080/14634988.2016.1208028>
- 560 Su, D., Lin, P., Mao, H., Wu, J., Liu, H., Cui, Y., Qiu, C. Features of slope intrusion mesoscale
561 eddies in the northern South China Sea. *Journal of Geophysical Research: Oceans*, 2020, 125,
562 e2019JC015349. <https://doi.org/10.1029/2019JC015349>.
- 563 Tang, H., Shu, Y., Wang, D., Xie, Q., Zhang, Z., Li, J., Shang, X., Zhang, O., Liu, D. Submesoscale
564 processes observed by high-frequency float in the western South China Sea. *Deep Sea*
565 *Research Part I: Oceanographic Research Papers*, 2022, 103896.
566 <https://doi.org/10.1016/j.dsr.2022.103896>
- 567 Thomas, L., Taylor, J., Ferrari, R., Terrence M. Symmetric instability in the Gulf Stream. *Deep Sea*
568 *Research Part II: Topical Studies in Oceanography*, 2013, 91, 96–110.
569 <https://doi.org/10.1016/j.dsr2.2013.02.025>
- 570 Todd, R.E., Ren, A.S. Warming and lateral shift of the Gulf Stream from in situ observations since
571 2001. *Nature Climate Change*, 2023, 13, 1348–1352. [https://doi.org/10.1038/s41558-023-](https://doi.org/10.1038/s41558-023-01835-w)
572 [01835-w](https://doi.org/10.1038/s41558-023-01835-w)
- 573 Wang, G., Su, J., Chu, P. Mesoscale eddies in the South China Sea observed with altimetry.
574 *Geophysical Research Letter*, 2003, 30(21), 2121. doi: 10.1029/2003GL018532.
- 575 Wang, G., Chen, D., Su, J. Winter eddy genesis in the eastern South China Sea due to orographic
576 wind jets. *Journal of Physical Oceanography*, 2008, 38(3), 726–732.
577 <https://doi.org/10.1175/2007jpo3868.1>
- 578 Wang, Q., Zeng, L., Li, J., Chen, J., He, Y., Yao, J., Wang, D., Zhou, W. Observed Cross-Shelf Flow
579 Induced by Mesoscale Eddies in the Northern South China Sea. *Journal of Physical*
580 *Oceanography*, 2018, 48, 1609–1628. <https://doi.org/10.1175/JPO-D-17-0180.1>
- 581 Wang, D., Xu, H., Lin, J., Hu, J. Anticyclonic eddies in the northeastern South China Sea during
582 winter of 2003/2004. *Journal of Oceanography*, 2008, 64(6), 925–935
- 583 Wang, Z., Chen, Q. Warm core eddies in the northern South China Sea (I): Preliminary observations
584 of warm eddies in the South China Sea. *Journal of Oceanography of Taiwan Strait*, 1987, 18,
585 92–103.
- 586 Xu, J., Su, J. Hydrographic analysis of Kuroshio intrusion into the South China Sea II: Observations
587 during ~~Aug~~UGust-September 1994. *Tropical Oceanography*, 1997, 2, 1–23.
- 588 Yang, H., Liu, Q. The seasonal features of temperature distributions in the upper layer of the South
589 China Sea. *Oceanologia et Limnologia Sinica*, 1998, 29(5), 501–507.
- 590 Xiu, P., Chai, F., Shi, L., Xue, H., Chao, Y. A census of eddy activities in the South China Sea during
591 1993–2007. *Journal of Geophysical Research: Oceans*, 2010, 115, C03012. doi:
592 10.1029/2009JC005657.
- 593 Yang, Q., Nikurashin, M., Sasaki, H., Sun, H., Tian, J. Dissipation of mesoscale eddies and its
594 contribution to mixing in the northern South China Sea. *Scientific Reports*, 2019, 9,
595 <https://doi.org/10.1038/s41598-018-36610-x>
- 596 Yi, Z., Wang, D., Qiu, C., Mao, H., Yu, J., Lian, S. Variations in dissolved oxygen induced by a
597 tropical storm within an anticyclone in the Northern South China Sea. *Journal of Ocean*
598 *University of China*, 2022, 21(5), 1084–1098. <https://doi.org/10.1007/s11802-022-4992-4>.

599 Zhang, Z., Qiu, B. Evolution of submesoscale ageostrophic motions through the life cycle of oceanic
600 mesoscale eddies. *Geophysical Research Letters*, 2018, 45(21), 11847-11855.
601 <https://doi.org/10.1029/2018GL080399>

602 Zhang, Z., Tian, J., Qiu, B., Zhao, W., Chang, P., Wu, D. Observed 3D Structure, Generation, and
603 Dissipation of Oceanic Mesoscale Eddies in the South China Sea. *Scientific Reports*, 2016,
604 6(1), 24349. <https://doi.org/10.1038/srep24349>

605 Zhang, Z., Zhao, W., Qiu, B., Tian, J. Anticyclonic eddy sheddings from Kuroshio loop and the
606 accompanying cyclonic eddy in the Northeastern South China Sea. *Journal of Physical*
607 *Oceanography*, 2017, 47(6), 1243-1259. <https://doi.org/10.1175/JPO-D-16-0185.1>

608